24th COBEM - 2017

24th ABCM International Congress of Mechanical Engineering
December 3-8, 2017, Curitiba, PR, Brazil

COBEM-2017-0838
ANALYSIS OF PIEZOELECTRIC SENSOR NETWORKS FOR SPATIAL MODAL FILTERS AND ACTIVE VIBRATION CONTROL

Filipe Moraes Horiy
Augusto Hirao Shigueoka
Marcelo Areias Trindade
São Carlos School of Engineering, University of São Paulo, Av. Trabalhador São-Carlense, 400, São Carlos, SP 13566-590, Brazil
filipehoriy@usp.br; augusto.shigueoka@usp.br; trindade@sc.usp.br

Abstract. *This work presents an analysis of a regular network of piezoelectric sensors and actuators on a rectangular plate and its application to a non-collocated active vibration control using a feedback of a signal obtained from a weighted-sum of the signals from the sensors in the network. Two methodologies are considered to combine the sensors signals. The first is based on the concept of spatial modal filters in which the combined signal is built to approximate a mono-modal response. This leads to the evaluation of the weighting of each sensor signal using the inversion of the Frequency Response Function matrix through a LSQ method. The second technique consists on the search for the weighting of the sensors signals that minimizes a closed-loop cost function, considering a direct derivative feedback, through a genetic algorithm optimization method. For that, an electromechanically coupled finite element model of the plate with bonded piezoceramic patches is considered. Results have shown that it is possible to obtain a very good closed-loop performance, although within a limited frequency band, by using these techniques. As expected, the optimization based on the closed-loop response provided better results.*

Keywords: *vibration control, sensor networks, spatial modal filters, piezoelectric materials*

1. INTRODUCTION

The study of techniques for vibration control has attracted great interest, from civil engineering to aerospace engineering problems. This is due to the fact that in many cases structures are subject to excitations that induce undesired vibration and noise that can lead to structural damage, user comfort decrease, among other factors. Therefore, a system of compensation of perturbations, which is nothing more than the search to maintain a system in a given state responding to the external disturbances that try to move it of the desired state, is required. Thus, the approach of a compensation control system through a simple structure will enable a study of the efficiency of the use of active control through a network of sensors and piezoelectric actuators.

For cases where the focus lies on the attenuation of specific low-frequency vibration or sound radiation modes, the control performance can be substantially improved whenever it is possible to focus the control effort on these specific modes (Meirovitch and Baruh, 1982; Baz and Poh, 1990; Shelley, 1991; Preumont *et al.*, 2003). One such strategy put-forward in some works is based on the development of spatial modal filters, such that the signals of the sensors in a network are combined to approximate the response of a selected mode-equivalent system, in which the contribution of undesired modes is excluded. By doing this, a feedback of such combined (or filtered) signal could lead to a focus of the control effort on the modes of interest and also would not affect the undesired modes. Actually, there are two main ways to achieve spatial modal filters: (i) discrete sensor arrays and (ii) continuous distributed sensors. Discrete sensor arrays may include accelerometers, strain gauges, piezoelectric patches etc, whereas continuous distributed sensors may consist of piezoelectric films or optical fibers (Lee and Moon, 1990; Fripp and Atalla, 2001; Preumont *et al.*, 2003). Discrete sensor arrays or networks may be built using piezoelectric patches that are distributed in a host structure and whose measured signals may be combined through a specific weighted-sum in order to approximate the response of a desired vibration mode. Several methodologies have been used for the evaluation of the weighting coefficients for the output signals measured by an array of sensors. They can be divided in three groups: target modes output match, optimization techniques and frequency response function (FRF) matrix inversion (Fripp and Atalla, 2001; Pagani *et al.*, 2011). For the method based on the inversion of the FRF matrix, the latter may be either predicted by a numerical model (Chen and Shen, 1997) or experimentally measured (Shelley, 1991), in order to shape the target filtered response (Preumont *et al.*, 2003; Pagani and Trindade, 2009; Trindade *et al.*, 2015).

The use of any of the three methodologies for calculating the weighting coefficients can generate high performance modal filters, but generally this will be for a given frequency range. However, (Preumont *et al.*, 2003) stated that the

number of sensors required in the network should be at least the number of modes present in the frequency band of interest. Then, (Pagani and Trindade, 2009), have shown that is possible to decrease the number of required sensors by optimizing their locations. In any case, however, for practical applications in which the modal filter is not perfect, some further digital filtering could be required (Trindade *et al.*, 2015). Another strategy is to search for sensors signal weights that optimize the closed-loop response according to a given cost function (Shigueoka, 2015). Using this approach, the corresponding combined signal may not be related to that of a modal filter but its response is such that when fed back through the control actuators, the closed-loop response is improved.

In this work, the abovementioned two strategies to evaluate the weights of the sensors signals in a network are applied to the problem of active vibration control of a plate with a network of piezoceramic patches, some acting as sensors and others as actuators. The main objetive is to compare the performance of the strategies and to assess their frequency range limitations.

2. PROBLEM DESCRIPTION

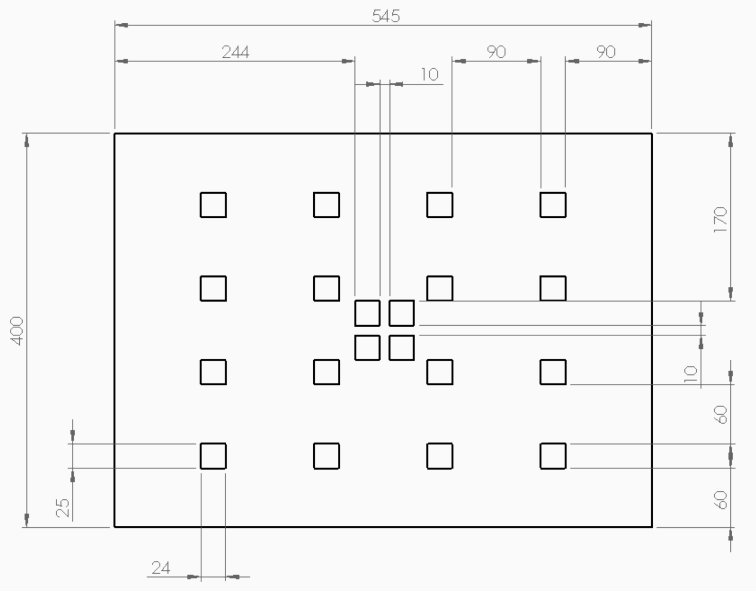

Figure 1. Configuration of piezoelectric patches $24{\times}25\mathrm{mm}$ – regular network four by four sensors and four actuators in the center – on aluminum plate with dimensions $545{\times}400{\times}3\mathrm{mm}$.

The network configuration of sensors and actuators that would be bonded to the plate (aluminum plate with dimensions $545{\times}400{\times}3\mathrm{mm}$, density of $2700\,\mathrm{kg/m^3}$, Young module of $69\,\mathrm{GPa}$, Poisson's ratio 0.33, and clamped at all edges) was the first step to be defined. Since we had 20 piezoelectric patches PZT5H, $24{\times}25\mathrm{mm}$, a regular network four by four of sensors and four more actuators was the most practical configuration for the use of all the patches (the configuration of the patches on the plate with the appropriate dimensions can be seen in Fig. 1). There is also a point located at $(\,235,\,158\,)\,\mathrm{mm}$, where an external normal force excitation will be applied. Measurement of displacement velocity will also be taken there. In later sections, such point will be identified as point P. For illustration, the already built plate with bonded piezoceramic patches used as base for the developed model is shown in Fig. 2.

3. METHODOLOGY

3.1 Optimization framework

When the piezoelectric patches are previously defined and positioned, the design of a discrete modal sensor is reduced to the problem of finding the α_j gains that will best serve its purpose. Multiple methods may be used (Friswell, 2001), all of which will ultimately give a $\boldsymbol{\alpha}$ vector of real parameters. Then, the performance of a system that uses the modal filter defined by $\boldsymbol{\alpha}$ may be evaluated by an objective function irrespectively of the nature of the optimization method that was employed. This way, it is possible to stablish a common criteria to compare numerous alternatives to compute $\boldsymbol{\alpha}$. In this work, in particular, two different methods were used to compute $\boldsymbol{\alpha}$: pseudo-inverse and genetic algorithm. Once a set of values for $\boldsymbol{\alpha}$ is found, the performance of the closed-loop system is checked by computing the performance index as explained in the following section.

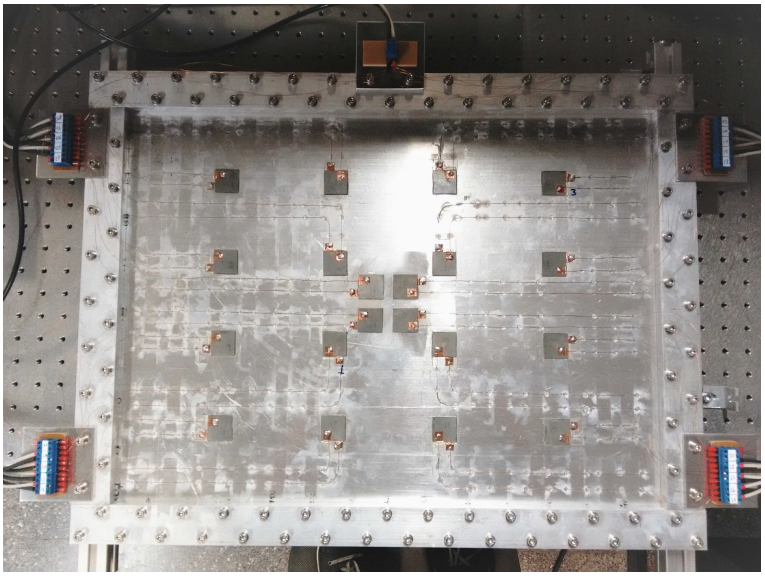

Figure 2. Set plate plus piezoelectric patches fixed on an inertial table.

3.2 Measuring the closed-loop performance

Starting from a finite element model for the structure with piezoelectric patches, detailed in (Santos, 2012), with mechanical displacements and electric charges at patches as degrees of freedom, the electromechanical coupled equations of motion read

$$\begin{bmatrix} \boldsymbol{M} & \mathbf{0} & \mathbf{0} \\ \mathbf{0} & \mathbf{0} & \mathbf{0} \\ \mathbf{0} & \mathbf{0} & \mathbf{0} \end{bmatrix} \begin{bmatrix} \ddot{\boldsymbol{u}} \\ \ddot{\boldsymbol{q}}_s \\ \ddot{\boldsymbol{q}}_a \end{bmatrix} + \begin{bmatrix} \boldsymbol{K}_u & -\boldsymbol{K}_{uqs} & -\boldsymbol{K}_{uqa} \\ -\boldsymbol{K}_{uqs}^T & -\boldsymbol{K}_{qs} & 0 \\ -\boldsymbol{K}_{uqa}^T & 0 & -\boldsymbol{K}_{qa} \end{bmatrix} \begin{bmatrix} \boldsymbol{u} \\ \boldsymbol{q}_s \\ \boldsymbol{q}_a \end{bmatrix} = \begin{bmatrix} \boldsymbol{f}(t) \\ \boldsymbol{V}_s(t) \\ V_a(t) \end{bmatrix}, \tag{1}$$

where, $\boldsymbol{M}$ is the inertia matrix; $\boldsymbol{K}_u$ is the mechanical stiffness matrix; $\boldsymbol{K}_{qs}$ and $\boldsymbol{K}_{qa}$ are dielectric stiffness matrices of sensors and actuators; $\boldsymbol{K}_{uqs}$ and $\boldsymbol{K}_{uqa}$ are piezoelectric stiffness matrices; $\boldsymbol{u}$ is a vector containing mechanical degrees of freedom; $\boldsymbol{q}_s$ and $\boldsymbol{q}_a$ are vectors containing electrical charges degrees of freedom; $\boldsymbol{f(t)}$ is an external force being applied on point P; $\boldsymbol{V}_s(t)$ is a vector of electrical voltages induced in the sensors; $V_a(t)$ is the prescribed voltage applied to the actuating patches.

It is customary practice to work in modal coordinates and perform modal projection in order to simplify the matrices in the dynamic equation and also reduce the order of the model, thus greatly reducing computational costs with no significant impact on accuracy (Meirovitch, 1980). Assuming that those transformations and static condensation for the sensors' voltages have already been applied, the equations of motion for the first m vibration modes are rewritten as

$$\ddot{\boldsymbol{\eta}} + \boldsymbol{\Lambda}\dot{\boldsymbol{\eta}} + \boldsymbol{\Omega}^2\boldsymbol{\eta} = \boldsymbol{\Phi}^T\boldsymbol{f}(t) + \boldsymbol{\Phi}^T\boldsymbol{K}_{uva}V_a \tag{2}$$

$$\boldsymbol{V}_s = -\boldsymbol{K}_{uqs}^T\boldsymbol{\Phi}\boldsymbol{\eta}, \tag{3}$$

where $\boldsymbol{\Lambda}$ is a matrix of modal damping; $\boldsymbol{\Omega}^2$ is a diagonal matrix whose elements are the square of the natural frequencies; $\boldsymbol{\Phi}$ is a matrix whose columns are the eigenvectors associated to the m first vibration modes normalized such that $\boldsymbol{\Phi}^T\boldsymbol{M}\boldsymbol{\Phi} = \boldsymbol{I}$, where $\boldsymbol{I}$ is the identity matrix. The vector $\boldsymbol{\eta}$ is obtained from the transformation $\boldsymbol{u} = \boldsymbol{\Phi}\boldsymbol{\eta}$. By defining the state vector as $\boldsymbol{z} = [\,\boldsymbol{\eta}\;\;\dot{\boldsymbol{\eta}}\,]^T$, it is possible to rewrite the system equations as

$$\dot{\boldsymbol{z}} = \boldsymbol{A}\boldsymbol{z} + \boldsymbol{B}_f\boldsymbol{f}(t) + \boldsymbol{B}_aV_a(t) \tag{4}$$

$$u_p = \begin{bmatrix} \boldsymbol{C}_u\boldsymbol{\Phi} & \mathbf{0} \end{bmatrix}\boldsymbol{z} \tag{5}$$

$$y = \dot{u}_p = \begin{bmatrix} \mathbf{0} & \boldsymbol{C}_u\boldsymbol{\Phi} \end{bmatrix}\boldsymbol{z} = \boldsymbol{C}_y\boldsymbol{z} \tag{6}$$

$$\boldsymbol{V}_s = \begin{bmatrix} \boldsymbol{K}_{uqs}^T\boldsymbol{\Phi} & \mathbf{0} \end{bmatrix}\boldsymbol{z} \tag{7}$$

$$\dot{\boldsymbol{V}}_s = \begin{bmatrix} \mathbf{0} & \boldsymbol{K}_{uqs}^T\boldsymbol{\Phi} \end{bmatrix}\boldsymbol{z} = \boldsymbol{C}_{dvs}\boldsymbol{z}, \tag{8}$$

with subindex P indicating measurements taken at point P. The output of the modal filter is, according to its definition,

$$V_f(t) = \boldsymbol{\alpha}^T\boldsymbol{V}_s. \tag{9}$$

The control law of the form

$$V_a(t) = -K\dot{V}_f = -K\boldsymbol{\alpha}^T\dot{\boldsymbol{V}}_s. \tag{10}$$

By using Eqs. (4), (8), (9) and (10), it is possible to arrive at the state-space formulation of the closed-loop system

$$\dot{\boldsymbol{z}} = (\boldsymbol{A} - K\boldsymbol{B}_a\boldsymbol{\alpha}^T\boldsymbol{C}_{dvs})\boldsymbol{z} + \boldsymbol{B}_f\boldsymbol{f}(t). \tag{11}$$

By taking the Laplace Transform of Eq. (11) and isolating $\boldsymbol{z}$, one gets

$$\boldsymbol{z}(s) = (\boldsymbol{I}s - \boldsymbol{A} + K\boldsymbol{B}_a\boldsymbol{\alpha}^T\boldsymbol{C}_{dvs})^{-1}\boldsymbol{B}_f f(s). \tag{12}$$

The closed-loop displacement velocity measured at point P and the control effort may then be calculated by combining Eqs. (12), (6), (8) and (10), resulting in

$$y(s) = \boldsymbol{C}_y(\boldsymbol{I}s - \boldsymbol{A} + K\boldsymbol{B}_a\boldsymbol{\alpha}^T\boldsymbol{C}_{dvs})^{-1}\boldsymbol{B}_f f(s) = H_{ys}(s)f(s) \tag{13}$$

$$V_a(s) = -K\boldsymbol{\alpha}^T\boldsymbol{C}_{dvs}(\boldsymbol{I}s - \boldsymbol{A} + K\boldsymbol{B}_a\boldsymbol{\alpha}^T\boldsymbol{C}_{dvs})^{-1}\boldsymbol{B}_f f(s) = H_{vaf}(s)f(s). \tag{14}$$

Thus the FRF with force input $f(\omega)$ and displacement velocity output $y(\omega)$, hereinafter denominated H_{yf}, may be found by evaluating Eq. (13) after applying the transformation $s = i\omega$ over the desired frequency range. Likewise, the FRF of the force input $f(s)$ and control effort output $V_a(s)$, henceforth denominated H_{vaf}, may be found after following the same procedure with Eq. (14).

It would be desirable to keep at minimun the maximum amplitude of both $y(\omega)$ and $V_a(\omega)$, but these quantities are inversely related, that is, one increases whenever the other decreases. The designer consequently has to choose a compromise between performance and control effort. In order to quantify vibration attenuation in each mode, the following metric J_Q was stablished:

$$J_Q = \sum_{j=1}^{m} W_j \, |H_{yf}(\omega_{r,j})|, \tag{15}$$

where W is a m-vector of weighting coefficients and $\omega_{r,j}$ is the resonance frequency (damped natural frequency) of the j-th mode. Thus J_Q is a weighted sum of all the peaks of the FRF H_{yf}. This study will use J_Q as a measure of performance, where lower values of J_Q mean better vibration attenuation.

3.3 Design of the optimal feedback control gain K

The previous section defined a way to measure the closed-loop performance, but did not specify $\boldsymbol{\alpha}$ nor K. This section describes the procedure for finding K, while the next sections will describe two methods used to find $\boldsymbol{\alpha}$.

The open-loop system, that is, with null feedback gain $K = 0$, will have the structure's natural damping and the control effort will be null, as no control feedback is being used. Thus, when $K = 0$ the system is always feasible. One can then increase K until either the damping or the control effort (or both) is violated. At this point, the search halts and the greatest feasible gain is taken as the optimal feedback gain for the DVF control law. The procedure used here is then as follows: if the closed-loop system has acceptable damping and control effort not above the stipulated limit, then make the performance index J defined to be equal to J_Q, as defined in Eq. (15). Otherwise, it is defined to be an extremely high value, which in this study was set to 1×10^6. In this study,

$$J = \begin{cases} J_Q & \text{if } \xi_j > 0.25\% \quad \text{and} \quad \max\limits_{100\,\text{Hz} \le r \le 2100\,\text{Hz}} \dfrac{V_a}{f}(2\pi r) \le 200\text{V/N} \\ 1 \times 10^6 & \text{otherwise} \end{cases} \tag{16}$$

Note that a linear search is considerably costly, specially if K is to be computed within a low tolerance, since the number of iterations grows at order $O(10^n)$, where n is the number of significant digits. In this work, dichotomy search (Rao, 2009) was used as the computational complexity grows linearly with the number of significant digits, at order $O(n)$.

3.4 Design of the weighting coefficients α using least-squares (LSQ)

The first method for determining the weighting coefficients is based on the knowledge of the FRF of each sensor in the network and the natural frequencies of the target vibration modes. For that, the finite element model was used to perform a modal analysis and to evaluate the FRF measured by each piezoelectric sensor. Then, a target FRF is defined by considering an equivalent system of one degree of freedom with natural frequency Ω_j and damping factor ξ_j such that

$$g_j(\omega) = \frac{2\xi_j\omega_j^2}{\omega_j^2 - \omega^2 + 2i\xi_j\omega_j\omega} \tag{17}$$

Equation (17) represents a realistic objective for the filtered FRF signal if the resonance peaks are well defined. And for a frequency domain $[\omega_1, \ldots, \omega_m]$ using a matrix Y that represent the FRF of the n selected sensors in the array in the same domain and using the vector of coefficients α_j which equates the filtered output (weighted sum of sensors outputs).

$$\begin{bmatrix} Y_1(\omega_1) & Y_2(\omega_1) & \cdots & Y_n(\omega_1) \\ Y_1(\omega_2) & Y_2(\omega_2) & \cdots & Y_n(\omega_2) \\ \vdots & \vdots & \ddots & \vdots \\ Y_1(\omega_m) & Y_2(\omega_m) & \cdots & Y_n(\omega_m) \end{bmatrix} \begin{bmatrix} \alpha_{j1} \\ \alpha_{j2} \\ \vdots \\ \alpha_{jn} \end{bmatrix} = \begin{bmatrix} g_j(\omega_1) \\ g_j(\omega_2) \\ \vdots \\ g_j(\omega_m) \end{bmatrix} \tag{18}$$

According to (Pagani *et al.*, 2011), the linear system defined by Eq. (18) in general admits only approximate solutions, which will be denoted $\boldsymbol{\alpha}^*$. The vector of weighting coefficients $\boldsymbol{\alpha}^*$ represents the best solution, in the least-squares sense, for the design of a modal filter which isolates the j-th vibration mode response. If several vibration modes are to be considered simultaneously as target modes for the filter design, it is necessary to define G as the matrix of target FRFs with dimension $m \times p$, where p denotes the number of target modes. Consequently, the approximate solution $\boldsymbol{\alpha}^*$ of Eq. (18) is a matrix of dimension $n \times p$, that is, one column vector of weighting coefficients for each one of the target modes. This may be written in a compact form as

$$\boldsymbol{Y}\boldsymbol{\alpha}^* = \boldsymbol{G} \tag{19}$$

However, $\boldsymbol{Y}\boldsymbol{\alpha}^*$ is an approximation of $\boldsymbol{G}$, since its elements are the result of an orthogonal projection of the columns of $\boldsymbol{G}$ for the space covered by the columns of $\boldsymbol{Y}$. The solution of Eq. (19) can be obtained by traditional Moore-Penrose pseudo-inverse solution multiplying it by $\boldsymbol{Y}^H$,

$$\boldsymbol{Y}^H\boldsymbol{Y}\boldsymbol{\alpha}^* = \boldsymbol{Y}^H\boldsymbol{G}, \tag{20}$$

such that

$$\boldsymbol{\alpha}^* = \left(\boldsymbol{Y}^H\boldsymbol{Y}\right)^{-1}\boldsymbol{Y}^H\boldsymbol{G} \tag{21}$$

Still according to (Pagani *et al.*, 2011), the inversion of $\boldsymbol{Y}^H\boldsymbol{Y}$ is unnecessary and computationally inefficient (for a full column rank matrix), since $\boldsymbol{Y}$ may be decomposed through QR decomposition, where $\boldsymbol{Q}$ is an orthonormal matrix and $\boldsymbol{R}$ is upper triangular, such that $\boldsymbol{Y} = \boldsymbol{Q}\boldsymbol{R}$ and Eq. (21) can be rewritten, after an expansion and accounting for $\boldsymbol{Q}^H\boldsymbol{Q} = \boldsymbol{I}$, as

$$\boldsymbol{\alpha}^* = \boldsymbol{R}^{-1}\boldsymbol{Q}^H\boldsymbol{G} \tag{22}$$

The QR decomposition method was one of the methods employed in this work being convenient for the cases in which the FRF matrix has had full column rank.

3.5 Design of the weighting coefficients α using Genetic Algorithm (GA)

The second method for determining the weighting coeffcients is based on a direct search using genetic algorithm, which is an evolutive computation method based on a population that undergoes successive applications of mainly two operations, crossover and mutation, that will search the best individual. Each individual in a population is an instance of the design parameters. In the present case, one individual is a set of weighting coefficients $\boldsymbol{\alpha}$, whose probability of survival in the population depends on how well it scores with the objective function. For such set $\boldsymbol{\alpha}$, K is calculated according to the procedure described in sub-section 3.3. The fitness of the individual is then set to be equal to the performance index J used to find the optimal K.

4. RESULTS

The numerical analysis was divided into three parts: (i) modal analysis of the plate to determine vibration modes that could contribute the most to acoustic radiation, their natural frequencies and electric potential induced in the patches; (ii) assessment of the closed-loop performance when considering the two methods (LSQ and GA) and for different frequency ranges; (iii) comparison between closed-loop performances of the two methods for selected frequency ranges.

Figure 3 shows the vibration modes and natural frequencies. For each mode, the electric potentials induced in the 16 sensor patches and 4 actuator patches are also shown, from which it is possible to assess the modal contribution of the each patch. Based on the represented induced electric potential in the patches, the mode shapes also indicate that, from the first ten modes, the first, fourth and eighth could contribute the most for acoustic radiation and, therefore, are selected as target for the active vibration control.

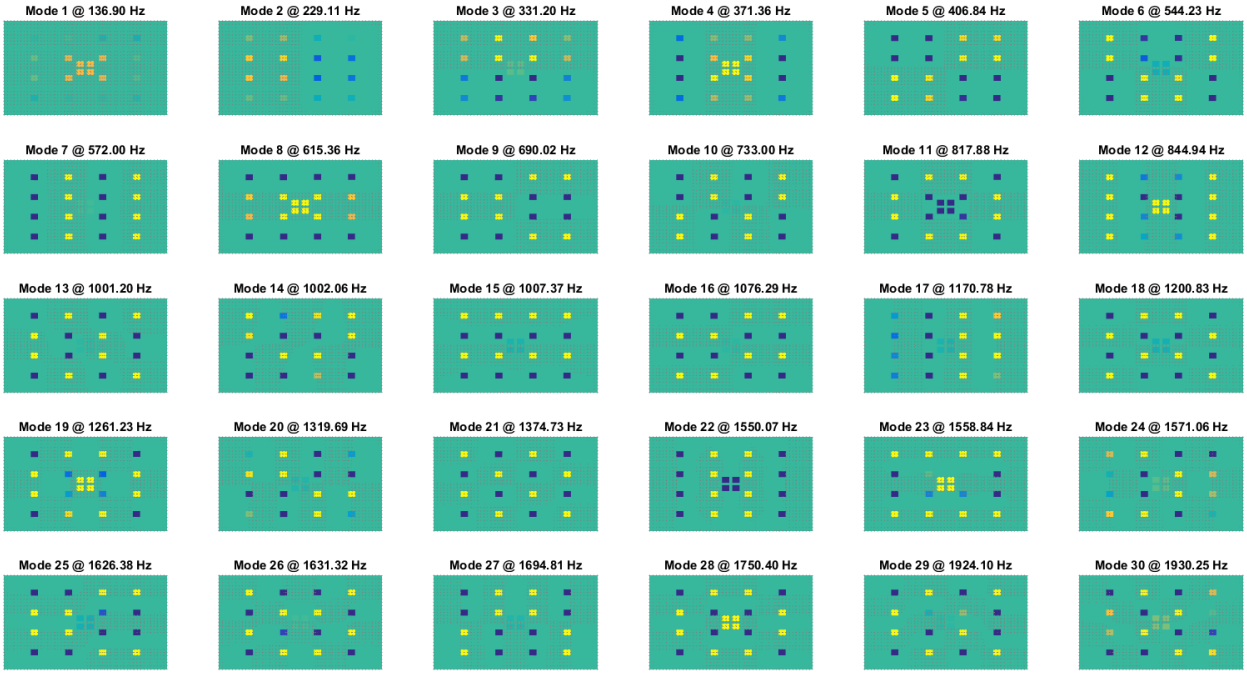

Figure 3. Vibration modes of a clamped rectangular plate with 20 piezoelectric patches.

4.1 Comparison between the optimum from LSQ and from GA

After having fixed the target functions g_j, the correspoding modal sensors were designed at first using the Moore-Penrose pseudo-inverse. Since such method actually solves the associated least-squares problem, it will henceforth be denominated LSQ in the following graphs. Afterwards, another design was also made, only that this time the α_j gains were found by the genetic algorithm (GA) optimization as described above. Several first attempts on this optimization study indicated that increasing number of modes in the model generally has a detrimental effect on the success of both LSQ and GA in returning a design that can be used in vibration control. Therefore, the Pareto Front was computed for both methods in order to better appreciate the relationship between the number of modes in the model and the objective function $J(\boldsymbol{\alpha})$. Even though different optimization methods were employed, both LSQ and GA ultimately return the same type of result: the vector $\boldsymbol{\alpha}$ used in the modal sensor. Given that the objective function $J(\boldsymbol{\alpha})$, which measures the closed-loop performance of the derivative control, depends only on $\boldsymbol{\alpha}$, then it is possible evaluate the performance of each design using the same criteria and even compare the two Pareto Fronts in the same graph.

The fitness was then computed for each optimal found and plotted against the number of modes taken into account during optimization, (Figure 4). It is evident that, according to the objective function used in this formulation, GA always returned a design that in closed-loop scored better than the one obtained from LSQ. Besides, a closer inspection of Fig. 4 on the cases with 19, 20 or 21 modes reveals that the GA was able to keep the value of the objective function almost at the same level as the ones obtained with 16, 17 or 18 modes.

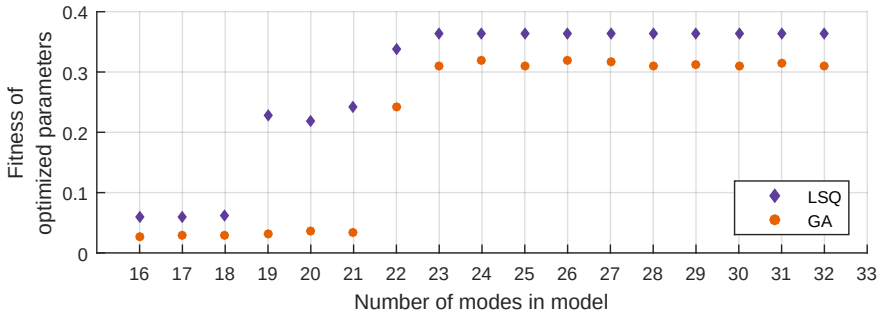

Figure 4. Pareto front of both LSQ and GA optimization methods, with fitness function on the vertical axes and number of modes taken into account during design on the horizontal axes.

The Pareto Fronts allowed for a general overview of the results, inasmuch specific as the information they provide. However, a better understanding of the phenomena underlying these results requires a more detailed investigation, so

Table 1. Comparison betwen the closed-loop performance of the modal sensors designed from LSQ or GA when used for vibration control in conjunction with DVF. The first 18 modes were considered.

		Peak atten. (dB)		Closed-loop ξ (%)	
Mode	ω_r (Hz)	LSQ	GA	LSQ	GA
1	136	19.5	29.0	4.71	13.32
2	228	0.3	−0.2	0.52	0.49
3	328	0.0	1.4	0.50	0.51
4	370	18.9	25.0	4.74	5.15
5	405	−0.8	−1.0	0.50	0.51
6	542	0.0	0.1	0.50	0.50
7	572	0.0	1.8	0.50	0.51
8	611	7.3	9.3	4.70	100.00
9	687	−2.1	−1.2	0.50	0.50
10	731	0.0	17.8	0.50	2.93
11	815	0.9	−10.8	0.50	0.48
12	843	0.3	21.7	0.50	0.42
13	998	0.2	0.2	0.51	0.40
14	999	0.2	0.8	0.48	0.49
15	1001	0.2	1.2	0.51	0.66
16	1070	−0.2	10.6	0.50	0.51
17	1167	0.0	2.0	0.50	0.55
18	1195	0.0	3.7	0.50	0.56

Table 2. Comparison betwen the closed-loop performance of the modal sensors designed from LSQ or GA when used for vibration control in conjunction with DVF. The first 21 modes were considered.

		Peak atten. (dB)		Closed-loop ξ %	
Mode	ω_r (Hz)	LSQ	GA	LSQ	GA
1	136	4.0	29.6	0.79	14.89
2	228	0.1	−0.1	0.51	0.50
3	328	0.0	1.3	0.50	0.52
4	370	3.8	18.8	0.79	4.38
5	405	−3.0	−0.7	0.49	0.50
6	542	0.0	−0.4	0.50	0.50
7	572	0.0	1.5	0.50	0.51
8	611	0.5	8.9	0.79	55.88
9	687	0.6	1.1	0.51	0.50
10	731	0.1	−0.4	0.50	0.50
11	815	−1.6	22.1	0.50	1.89
12	843	−1.8	3.2	0.50	0.28
13	998	−0.3	1.9	0.47	0.49
14	999	−0.1	2.4	0.48	0.47
15	1001	0.1	2.8	0.55	0.65
16	1070	0.1	4.5	0.50	0.52
17	1167	0.0	1.9	0.50	0.59
18	1195	0.0	1.6	0.50	0.53
19	1258	4.6	−0.7	0.50	0.53
20	1315	−3.3	0.6	0.50	0.50
21	1370	0.2	1.4	0.50	0.51

filtered frequency response obtained from LSQ and GA optimizations were compared against each other when considering 18 and 21 vibration modes in the optimization (Figure 5). Since only the relative values of the α_j coefficients are relevant, the graph considered $\boldsymbol{\alpha}$ normalized to 1. Notice that the LSQ-based modal filter shows only modes 1, 4 and 8, all in-phase, up to the frequency range considered (that includes only the first 18 natural frequencies). On the other hand, GA-based modal filter also shows modes 11, in-phase, and 12, out-of-phase. Is is also possible to observe that LSQ-based modal filter equalizes the peak amplitudes, while the GA-based one lead to peak amplitudes increasing with frequency.

Whether such difference is effective or not can be inferred from Fig. 6, where the FRF of force excitation and velocity measurement is taken at point P. While the LSQ modal filter leads to an attenuation of $20\,\mathrm{dB}$ in the 1st mode relative to

the open-loop FRF, the GA modal filter yields $30\,\mathrm{dB}$. Mode 11, which was not as penalized as modes 1, 4 and 8, also got attenuated as a collateral effect. In all other modes, the GA modal sensor is not significantly worse than the LSQ modal sensor. These results may be explained considering the control effort FRF shown in Fig. 7. It shows that the GA modal filter is able to better make use of the stipulated control voltage limit of $200\,\mathrm{V/N}$, which equals $46\,\mathrm{dB}$ (ref. $\mathrm{V/N}$) in the graph. The LSQ modal filter, on the other hand, saturates the control effort at the 2nd mode and, considering derivative control, prevents a higher gain, which would be beneficial to the 1st mode.

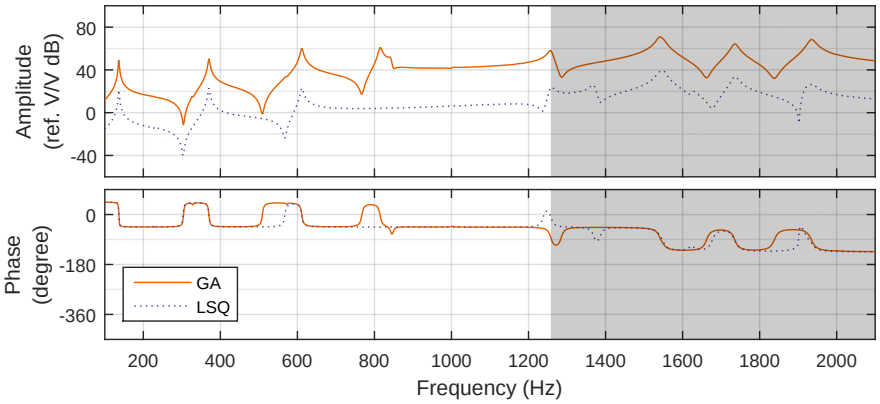

Figure 5. Frequency response of the modal filters optimized using LSQ and GA for the full 32-modes model, when considering only 18 modes in the filter optimization.

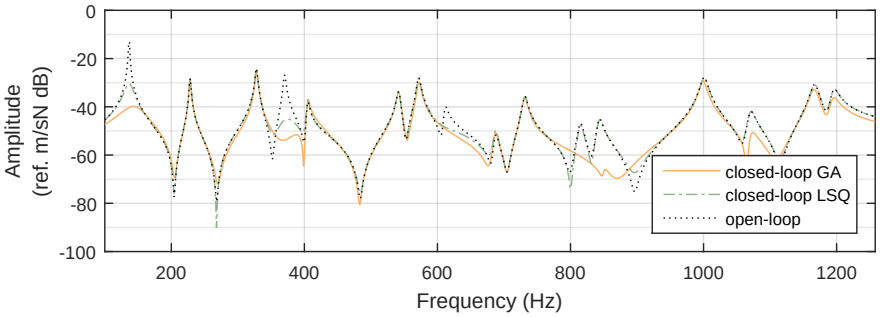

Figure 6. Comparison between the open-loop and the closed-loop mobility of point P

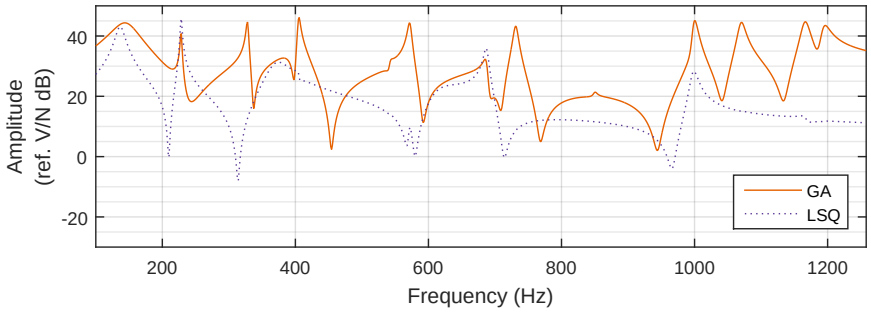

Figure 7. Comparison between control effort frequency response using LSQ-based and GA-based modal filters designed considering only the first 18 modes.

While in the previous case both LSQ-based and GA-based modal filters present satisfactory performance, when 21 modes are considered to design the filters, the difference between the two techniques becomes much more remarkable. The filtered frequency response of LSQ-based and GA-based modal filters are not so different (Fig. 8), with few other peaks appearing in the response. However, the comparison of the closed-loop FRF with force excitation and velocity measurement shows that the LSQ modal filter is ineffective in attenuating resonance peaks, while the performance of the GA-based modal filter is not seriously affected. The reason for this limitation is again explained by the control effort response shown in Fig. 10, where the control effort at mode 12 prevents the LSQ modal filter from effectively controlling target modes 1, 4 and 8.

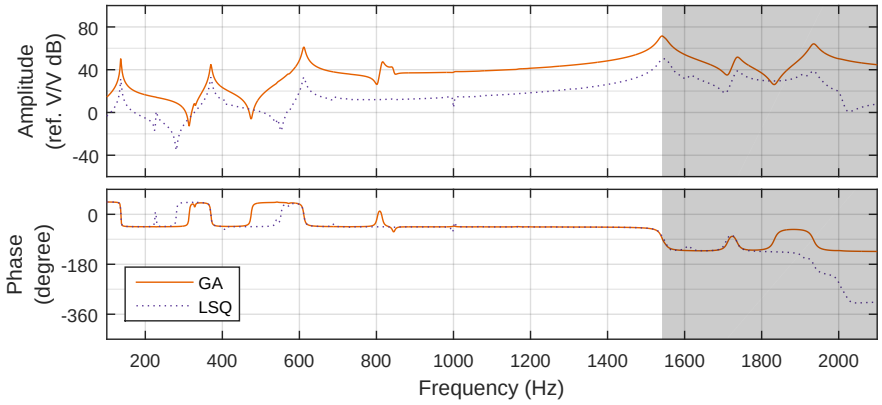

Figure 8. Frequency response of the modal filters optimized using LSQ and GA for the full 32-modes model, when considering only 21 modes in the filter optimization.

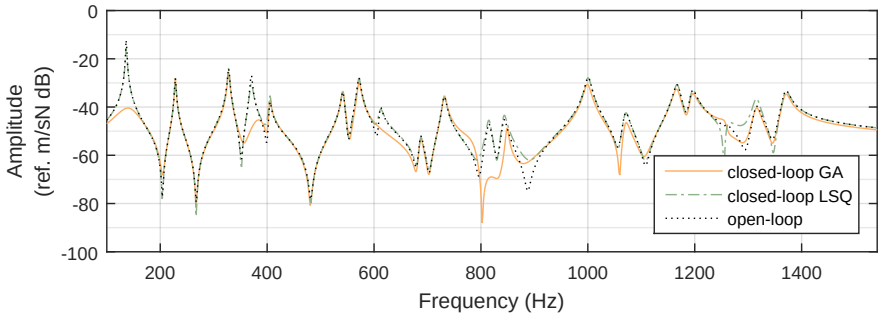

Figure 9. Comparison between the open-loop and the closed-loop mobility of point P.

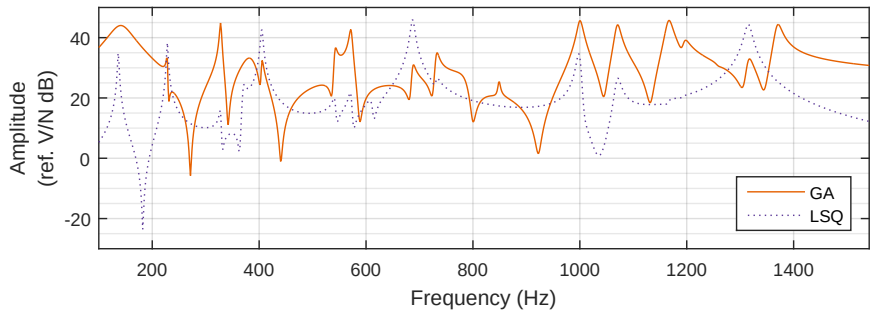

Figure 10. Comparison between the control effort frequency response using LSQ-based and GA-based modal filters designed considering only the first 21 modes.

4.2 Discussion on the optimality of LSQ

It is possible to deduce from the numerical results that the design of modal filters based on the Moore-Penrose pseudo-inverse as done in (Preumont *et al.*, 2003), while optimal in the least-squares sense for approximating a target function $g(\omega)$, may not yield a modal filter that is also optimal for vibration control. As seen from the results, the almost minimal-phase FRF obtained from the GA modal filter has more in-phase modes than expected, a trait which only increment the system dampening when using derivative control. Besides, the magnitude of the peaks are corrected so as to level the maximum control effort. According to the available literature, it is customary to only choose a target function $g(\omega)$ composed of modes of interest with unitary peaks. Any deviation, even a beneficial one, is penalized. Consequently, in the LSQ approach the designer would have to know *a priori* the modes which can be made in-phase and their peak magnitude. Finding those parameters is not a trivial task, which means that the LSQ method will not, in general, yield the optimal solution.

There is, though, one characteristic that both the optimal designs obtained from LSQ and from GA share: the minimal-phase FRF for the modal sensor. It may be profitable to investigate a non-GA method that will try to give the best minimal-phase approximation irrespective of a target funtion $g(\omega)$. This way, one could obtain a design which is almost as effective as the one obtained from GA with a lower computational cost.

5. CONCLUSIONS

This work presented two methodologies to design spatial modal filters aiming at satisfactory closed-loop performance when derivative feedback of the filtered response is considered. Results have shown that, for a limited frequency-range, LSQ-based modal filter, which can be designed in open-loop and, thus, is less expensive, may lead to satisfactory performance. In order to increase the frequency-range, though, the GA-based modal filter, which is designed in closed-loop and, thus, is more expensive, is required to guarantee satisfactory closed-loop performance. The latter allowed satisfactory performance up to 1500 Hz, which is a frequency range that contains the first 21 natural frequencies, using only 16 sensors. Experimental verification of these results are in progress.

6. ACKNOWLEDGEMENTS

Financial support of CAPES, through a Masters scholarship, and CNPq, through a Doctoral scholarship and research grants 574001/2008-5 and 309193/2014-1, is acknowledged.

7. REFERENCES

Baz, A. and Poh, S., 1990. "Experimental implementation of the modified independent modal space control method". *Journal of Sound and Vibration*, Vol. 139, pp. 133–149.

Chen, C.Q. and Shen, Y.P., 1997. "Optimal control of active structures with piezoelectric modal sensors and actuators". *Smart Materials and Structures*, Vol. 6, No. 4, pp. 403–409.

Fripp, M.L. and Atalla, M.J., 2001. "Review of modal sensing and actuation techniques". *The Shock and Vibration Digest*, Vol. 33, No. 1, pp. 3–14.

Friswell, M.I., 2001. "On the design of modal actuators and sensors". *Journal of Sound and Vibration*, Vol. 241, No. 3, pp. 361–372.

Lee, C.K. and Moon, F.C., 1990. "Modal sensors/actuators". *Journal of Applied Mechanics*, Vol. 57, No. 2, pp. 434–441.

Meirovitch, L., 1980. *Computational Methods in Structural Dynamics*. Springer Netherlands.

Meirovitch, L. and Baruh, H., 1982. "Control of self-adjoint distributed-parameter systems". *Journal of Guidance, Control, and Dynamics*, Vol. 5, No. 1, pp. 60–66.

Pagani, Jr, C.C. and Trindade, M.A., 2009. "Optimization of modal filters based on arrays of piezoelectric sensors". *Smart Materials and Structures*, Vol. 18, No. 9, pp. 1–12.

Pagani, Jr, C.C., Trindade, M.A. and Oliveira, L.P.R., 2011. "Experimental validation of modal filters based on arrays of piezoelectric sensors". In *Proceedings of the 21st International Congress of Mechanical Engineering*. Búzios.

Preumont, A., François, A., Man, P.D. and Piefort, V., 2003. "Spatial filters in structural control". *Journal of Sound and Vibration*, Vol. 265, No. 1, pp. 61–79.

Rao, S.S., 2009. *Engineering optimization: theory and practice*. Wiley, 4th edition.

Santos, H.F.L., 2012. *Controle ativo-passivo de vibrações estruturais suando materiais piezelétricos: otimização e quantificação de incertezas*. Ph.D. thesis, São Carlos School of Engineering, University of São Paulo, São Carlos, São Paulo.

Shelley, S.J., 1991. *Investigation of discrete modal filters for structural dynamic applications*. Ph.D. thesis, University of Cincinnati, Cincinnati.

Shigueoka, A.H., 2015. *Otimização de fitros modais espaciais usando redes de sensores aplicados ao controle de vibrações de estruturas do tipo viga e placa*. Master's thesis, São Carlos School of Engineering, University of São Paulo, São Carlos, São Paulo.

Trindade, M.A., Pagani, Jr, C.C. and Oliveira, L.P.R., 2015. "Semi-modal active vibration control of plates using discrete piezoelectric modal filters". *Journal of Sound and Vibration*, Vol. 351, No. 1, pp. 17–28.

8. RESPONSIBILITY NOTICE

The authors are the only responsible for the printed material included in this paper.